UCSF

Title

One-step optogenetics with multifunctional flexible polymer fibers

Permalink

https://escholarship.org/uc/item/1pr0v31f

Authors

Park, Seongjun
Guo, Yuanyuan
Jia, Xiaoting
et al.

Peer reviewed

One-Step Optogenetics with Multifunctional Flexible Polymer Fibers

Seongjun Park[1,2], **Yuanyuan Guo**[3,4,5], **Xiaoting Jia**[5], **Han Kyoung Choe**[6], **Benjamin Grena**[2,3], **Jeewoo Kang**[7], **Jiyeon Park**[8], **Chi Lu**[2,3], **Andres Canales**[2,3], **Ritchie Chen**[2,3], **Yeong Shin Yim**[6], **Gloria B. Choi**[6], **Yoel Fink**[2,3], and **Polina Anikeeva**[2,3,*]

[1]Department of Electrical Engineering and Computer Science, Massachusetts Institute of Technology, Cambridge, MA, USA

[2]Research Laboratory of Electronics, Massachusetts Institute of Technology, Cambridge, MA, USA

[3]Department of Material Science and Engineering, Massachusetts Institute of Technology, Cambridge, MA, USA

[4]Department of Biomedical Engineering, Tohoku University, Sendai, Miyagi, Japan

[5]Department of Electrical and Computer Engineering, Virginia Polytechnic Institute and State University, Blacksburg, VA, USA

[6]McGovern Institute for Brain Research Department of Brain and Cognitive Sciences, Massachusetts Institute of Technology, Cambridge, MA, USA

[7]Department of Chemical Engineering, Massachusetts Institute of Technology, Cambridge, MA, USA

[8]Department of Mechanical Engineering, Massachusetts Institute of Technology, Cambridge, MA, USA

Abstract

Optogenetic interrogation of neural pathways relies on delivery of light-sensitive opsins into tissue and subsequent optical illumination and electrical recording from the regions of interest. Despite the recent development of multifunctional neural probes, integration of these modalities within a

single biocompatible platform remains a challenge. Here, we introduce a device composed of an optical waveguide, six electrodes, and two microfluidic channels produced via fiber drawing. Our probes facilitated injections of viral vectors carrying opsin genes, while providing collocated neural recording and optical stimulation. The miniature (< 200 μm) footprint and modest weight (<0.5 g) of these probes allowed for multiple implantations into the mouse brain, which enabled opto-electrophysiological investigation of projections from the basolateral amygdala to the medial prefrontal cortex and ventral hippocampus during behavioral experiments. Fabricated solely from polymers and polymer composites, these flexible probes minimized tissue response to achieve chronic multimodal interrogation of brain circuits with high fidelity.

INTRODUCTION

With its genetic precision and millisecond resolution[1], optogenetics is an indispensable tool in neuroscience to correlate electrophysiological contributions of specific cell types to observed behaviors[2,3]. As this method depends on expression of light-sensitive microbial opsins in genetically identifiable neuronal populations[4], viral vectors must be infused directly into neural tissue. Opsins typically exhibit activation spectra in the visible range, where scattering properties of biological matter limit the penetration depth to <1mm[5], which necessitates implantation of light sources and additional hardware for electrophysiological readout. While significant progress has been made to engineer flexible[6], multifunctional and wireless probes with viral delivery and optical stimulation capabilities[7,8], integration of a recording functionality into these platforms continues to be a technological challenge. The development of such an integrated device is further complicated by the foreign body reaction to implanted probes, which stems from acute[9] and chronic[10] tissue damage that scale with the probe size and stiffness, respectively[11].

Here we develop miniature and flexible all-polymer integrated probes for behavioral optogenetic studies of neural circuits with reduced mechanical invasiveness. Our probes incorporate recording electrodes, optical waveguides, and microfluidic channels all within the dimensions of silica fibers routinely used in optogenetic experiments. To produce these probes, we rely on the thermal drawing process[12,13] that has previously facilitated fabrication of multifunctional devices for neural interfaces[14]. Our probes allowed for one-step surgery including injection of viral vectors carrying opsin genes into specific locations of the mouse brain and subsequent recording and optical stimulation of neural activity during free behavior. The small footprint of these devices permitted their implantation into several brain regions, facilitating optical control of behavior and electrophysiological readout of the underlying projection dynamics. With integrated modalities and a miniature footprint, this technology offers a minimally invasive alternative to multiple-step surgeries required for optogenetic mapping of brain function.

RESULTS

Design and fabrication of multifunctional fibers with engineered composite electrodes

Conductive polymers and polymer composites offer unmatched tunability in chemical and mechanical properties[15] allowing for precise engineering of materials interfaces with neural

tissue to achieve improved long-term recording performance compared to metallic electrodes[16,17]. These materials, however, often exhibit poor conductivity and are incompatible with high-throughput integration techniques[18]. Carbon-loaded polymer composites are characterized by high chemical stability in physiological solutions as well as tunable elastic properties[19,20]. The substantial sheet resistance of commercially available composites, however, restricts electrode miniaturization due to increased impedance, which reduces the ability of these electrodes to detect extracellular potentials.

To significantly improve electrode conductivity, we developed a custom conductive polymer composite comprised of conductive polyethylene (CPE) and 5 wt% graphite (Fig. 1a, gCPE). The sheet resistance of the composite was reduced by 4.1 times when compared to commercially available CPE (0.8 kΩ/γ for gCPE vs. 3.3 kΩ/γ for CPE). We hypothesized that the reduced sheet resistance should afford lower electrode dimensions without sacrificing the quality of electrophysiological recordings. Along with a waveguide core (polycarbonate (PC), refractive index n_{PC}=1.586, glass transition temperature T_g=150°C[21]) and cladding (cyclic olefin copolymer (COC), refractive index n_{COC}=1.53, T_g=158°C[22]), six gCPE electrodes (melting temperature T_M~123°C) were incorporated into a macroscopic template, a preform, by standard machining to produce a scaled-up version of the desired fiber (Fig. 1b). The preform was then heated and stretched into ~100 meter–long fiber with preform feature dimensions reduced by 50~200 times (Fig. 1c–e, Supplementary Fig. 1). By adjusting the drawing parameters, the sizes of electrodes and microfluidic channels were reduced to 20–30 μm, while the diameter of the waveguide was tuned between 50–80 μm. The entire integrated structure had a diameter between 180–220 μm. (Fig. 1f). For our experiments we have selected a fiber section with a diameter of 200 μm. Within this 10 meter long section the dimensions of the six electrodes were found to be 20.9±1.3 μm, 20.7±0.9 μm, 25.8±1.5 μm, 24.0±1.8 μm, 24.5±1.4 μm, and 22.6±2.3 μm; the microfluidic channels had dimensions of 16.4±2.1 μm and 15.3±1.9 μm; and the waveguide diameter measured 68.2±2.9 μm (Supplementary Fig. 1e).

Evaluation of mechanical, electrical, optical, and microfluidic properties of the fiber

The integrated fiber probes were flexible with a bending stiffness of 76.1–83.5 N/m in the frequency range of respiration and heartbeat (0.01–10 Hz), which is significantly lower than that of silica optical fibers (93.6–104.8 N/m) of comparable dimensions (Supplementary Fig. 2a). As neural interface devices are commonly fixed to the skull, the lower bending stiffness is anticipated to reduce the repeated tissue damage associated with relative motion of the brain with respect to the skull[23]. The impedance of multifunctional fiber electrodes at 1 kHz was found to be 1.31±0.27 MΩ, and could be further reduced to 0.62±0.23 MΩ by an overnight soak in a phosphate buffered saline (PBS) solution (Fig. 1g, h). Similar reduction to 0.67±0.12 MΩ was observed 3 days following implantation into the mouse brain, and the impedance remained consistent over 3 months (0.71±0.13 MΩ, Supplementary Fig. 2b). The observed decrease in impedance when compared to commercial CPE electrodes (2.10±0.39 MΩ/1.83±0.44 MΩ before/after soaking) could be attributed to the reduced sheet resistance and enhanced porosity of the composite electrodes (Supplementary Fig. 2c). Notably, the impedance of the composite gCPE electrodes was dominated by the tip geometry while the conductivity of the electrodes produced from commercial CPE was limited by sheet

resistance (Supplementary Fig. 2d). The impedance of the gCPE electrodes was invariant with respect to 90° bending deformation (Fig. 1g), and no current leakage through the polymer cladding (Supplementary Fig 2e, f) was observed. In addition, cyclic voltammetry curves of the gCPE electrodes exhibited capacitive behavior without any oxidation or reduction peaks within a voltage window exceeding the magnitude of extracellular potentials (Supplementary Fig 2g). The integrated waveguides exhibited relatively flat transmission in the visible spectrum, including the excitation peak of channelrhodopsin 2 (ChR2) at a wavelength λ=473 nm[24] (Supplementary Fig. 3a), as well as low transmission loss (< 1.5 dB/cm) (Supplementary Fig. 3b), which was maintained at body temperature (37 °C, Supplementary Fig. 3c, d), during bending deformation (90°–270° angles at radii of curvature 0.5–15 mm) and even following repeated bending cycles (Supplementary Fig. 3e, f). Transmission loss was also not affected by implantation into the mouse brain for up to 3 months (no longer time points were collected, Supplementary Fig. 3g). To confirm the utility of microfluidic channels for delivery of liquids into the brain tissue, a solution of a dye was infused into a brain phantom (0.6% agarose gel) (Fig. 1i). Return rate 70–95% of injected fluid at infusion speeds 1–100 nl/s was observed even during bending deformation (Fig. 1j). The maximum amount of fluid contained within a single microfluidic channel of 1 cm-long probe is 7.85 μl (which exceeds the volume of 3 μl that can be safely delivered into a mouse brain[25]), however unlimited amount can be delivered by connecting the channels to an external pump via miniature tubing.

Optogenetic interrogation of prefrontal cortex with multifunctional fibers

By integrating recording, optical stimulation, and microfluidic capabilities, our probe enabled multiple simultaneous experiments to be conducted following a one-step implantation surgery (Fig. 2a). The thermally drawn multifunctional fibers were outfitted with ferrules for optical coupling to lasers or light-emitting diodes, pin connectors for electrical readout, and tubing for fluid interfaces, respectively (Fig. 2b). The resulting probe weighed 0.3–0.5 g. To evaluate the ability of the fiber probes to mediate opto-electrophysiological interrogation of neural circuits, we implanted these devices into the medial prefrontal cortex (mPFC) of wild-type (WT) mice (Fig. 2c). There the integrated microfluidic channels were used to deliver an adeno-associated virus (AAV, serotype 5) carrying the gene for ChR2 fused to the enhanced yellow fluorescent protein (eYFP) under the excitatory neuronal promoter calmodulin kinase II α-subunit (*AAV5-CaMKIIa::ChR2-eYFP*) (Fig. 2d). Robust ChR2 expression in the mPFC was observed 2 weeks following the injection, and the extent of expression was proportional to the injection volume (Fig. 2e and Supplementary Fig. 4a, b). By combining the ability to deliver viral vectors through microfluidic channels and perform neural recording with gCPE electrodes during optical stimulation via integrated PC/COC waveguides, our probes provided an opportunity to investigate the temporal dynamics of the opsin expression in the mouse brain (Fig. 2f, Supplementary Table 1). To identify the onset of ChR2 expression following the injection of the AAV5 into the mPFC, electrophysiological signals were recorded in the presence of optogenetic stimulation (10 Hz, 8.6 mW/mm^2, 5 ms pulse width). For these stimulation parameters, which are common in optogenetics experiments, optically evoked potentials in the mPFC were observed following 11±2 days (n=8). As expected the amplitude of optically

evoked signal increased at larger optical powers and longer expression periods (Supplementary Fig. 4c).

Qualitatively similar optically evoked responses were found during acute recordings in transgenic Thy1-ChR2-YFP mice during optical stimulation at 10 Hz (Supplementary Fig. 5a–f). Stimulation at 100 Hz evoked activity uncorrelated with optical pulses, further confirming the physiological origin of the optically evoked potentials[26] (Supplementary Fig. 5g–l). As a third measure ensuring the physiological (rather than optical artifact) nature of our recordings, experiments in WT mice injected with a control virus *AAV5-CaMKIIa::eYFP* revealed no neural response to light pulses (Supplementary Fig. 6).

To illustrate the utility of the fiber probes for neurobiological experiments, WT mice implanted with fiber probes and transduced with *AAV5-CaMKIIa::ChR2-eYFP* or a control virus *AAV5-CaMKIIa::eYFP* in the mPFC were subjected to a standard open field test (OFT, 9 min session, 3 min light OFF/ON/OFF epochs) 6 weeks following surgery. Optical stimulation (5 ms pulse width, 16 mW/mm^2) in mPFC at 20 Hz and 130 Hz resulted in increased velocity (p < 0.05) in ChR2-expressing mice as compared to eYFP controls. (Fig 2g–j, Supplementary Video 1, 2). In agreement with prior experiments[27], there was no change in the time spent in the center of the open field for either group of mice (Supplementary Fig. 7a, b). In addition to the behavioral manifestation and electrophysiological readout, increased neuronal firing in ChR2-expressing mice was confirmed by the upregulation of an immediate early gene *c-fos* in the mPFC following optical stimulation. No *c-fos* upregulation was observed in control mice (Supplementary Fig. 7c–e).

Optical control and electrophysiological readout of projection dynamics with co-implanted fibers

Low footprint of the probes permitted their implantation into multiple brain targets and facilitated opto-electrophysiological projection mapping. In this study, one probe was implanted into the basolateral amygdala (BLA), where it was used for microfluidic delivery of *AAV5-CaMKIIa::ChR2-eYFP* or the control virus (*AAV5-CaMKIIa::eYFP*), and the second identical probe was implanted into either the mPFC[28,29] (Fig. 3a–d) or the ventral hippocampus (vHPC)[30] (Fig. 3e–h), which are known to receive excitatory projections from the BLA.

Similarly to the experiments in the mPFC, we have employed the fiber probes to identify the onset of functional ChR2 expression in the BLA and its projection targets (Supplementary Table 1). In the BLA, optically evoked (10 Hz, 8.6 mW/mm^2, 5 ms pulse width) neural activity emerged 11±2 days following AAV5 injection (n=8 mice, Fig. 3i). In the BLA-to-mPFC projection, optical stimulation evoked a low-latency (5 ms delay with respect to laser pulses) responses following 12±1 days (n=8 mice), and an additional response with a longer latency of 32 ms has emerged after 15±2 days (n=6 mice, Fig. 3j, Supplementary Fig. 8a, b). The evoked potentials with short latencies are consistent with direct axonal projections from the BLA to mPFC, while the long-latency activity may stem from a multi-synaptic network responses to optical stimulation in the mPFC[27]. In contrast to stimulation of the BLA inputs in the mPFC, optical excitation in the vHPC evoked only short-latency activity indicative of

direct axonal inputs from the BLA (Fig. 3k). This optically triggered activity could be measured 11 ± 2 days (n=8 mice) following AAV5 injection into the BLA. The faster onset of functional ChR2 expression in the BLA-to-vHPC as compared to BLA-to-mPFC projection could in part be explained by the shorter inter-region distance for the former projection. Similar to the recordings following the direct injection of the AAV5 into the mPFC, the amplitude of the ChR2-mediated signals in the BLA and its projection targets increased with optical power and period of expression (Supplementary Fig. 8c–e).

The observed electrophysiological response to optical stimulation of the BLA-to-vHPC projections was further correlated to the behavioral response observed in previous studies of this circuit[30]. Specifically, during the OFT (9-minute session, 3-minute OFF/ON/OFF epochs, Supplementary Video 3), mice transfected with ChR2 spent less time in the center of the open field during optical stimulation (20 Hz, 5ms pulse width) compared to the control group (Fig. 3l–n, $p < 0.05$). The total distance traveled and the average velocity, however, were not modulated by the optical stimulation (Supplementary Fig. 9a, b). An increase in *c-fos* expression was observed in the pyramidal layer of vHPC in ChR2-expressing mice whereas no change was found in the control group (Supplementary Fig. 9c–h). Consistent with stimulation of the vHPC, there was no significant change in neuronal *c-fos* level found in the BLA. To further confirm that the observed behavioral change in response to optical stimulation was a consequence of activation of BLA inputs in the vHPC, we employed fiber probes implanted in the vHPC to deliver AMPA receptor antagonist, synaptic blocker, 6-cyano-7-nitroquinoxaline-2,3-dione (CNQX). The dose of CNQX was first calibrated by simultaneously performing electrophysiological recording and optical stimulation during the infusion of the drug (Supplementary Fig. 10). Following CNQX infusion (0.5 μl, 0.1 mM) into the vHPC, optical stimulation of the BLA terminals did not result in behavioral changes, and ChR2-expressing mice were as likely to spend time in the center of the open field as the control mice during the light stimulation epoch (Fig 3o, $p = 0.2319$, Supplementary Video 4).

Assessment of chronic long-term performance and biocompatibility of fiber probes

As many neurobiological studies rely on being able to track the activity of identifiable neurons over the course of several weeks, we thought to investigate the ability of fiber probes to record isolated action potentials over a period of 3 months. We found that single neuron (unit) action potentials (spikes) can be isolated from our recordings using principle component analysis (PCA), and the spike shapes remain stable between 1 and 12 weeks (no longer time points were collected) following fiber probe implantation (Fig. 4a, b). For the representative units shown in Fig. 4a, b, separation between spike clusters was confirmed by calculating L-ratios, ($L_{ratio} < 0.01$ for all isolated units, Supplementary Table 2). Stability of the clusters was further confirmed by the analysis of the interspike interval (ISI) histograms (Fig. 4c, maximum interval 1000 ms, bin size 40 ms), as well as by calculating the average firing rates. The latter were found to be statistically different for the isolated units ($p < 0.001$, Fig. 4d). Supplementary Figure 11 contains PCA, ISI and firing rate analyses for additional isolated single units recorded from different mice over a period of 12 weeks. In addition to electrophysiological recording, the fiber probes maintained optical stimulation capability for up to 3 months (no longer time points were collected) with no significant

decrease in signal to noise ratio (4.7±0.8 for 1 month, 3.9±0.4 for 2 months, and 4.1±0.5 for 3 months, Fig. 4e–g).

We evaluated the biocompatibility of our all-polymer integrated fiber probes by immuno-histochemical quantification of markers characteristic of glial scarring (activated macrophage marker Iba1: ionized calcium-binding adaptor molecule 1, microglial marker ED1: cluster differentiation 68: CD68/macrosialin, astrocytic marker GFAP: glial fibrillary acidic protein) and chronic tissue damage associated with the breach of the blood-brain barrier (presence of Immunoglobulin G, IgG, in the brain tissue) in coronal brain slices (Fig 5, Supplementary Fig. 12)[11,31]. Compared to similarly sized insulated steel microwires (125 μm in diameter), the polymer fibers evoked significantly lower tissue response and blood-brain barrier breach 3 days following implantation ($p < 0.001$ for Iba1 and ED1, $p < 0.01$ for GFAP, and $p < 0.05$ for IgG). The attenuated levels of all markers were found for fiber probes implanted for up to 3 months, while significance persisted for the diminished presence of Iba1, GFAP ($p < 0.05$, up to 1 month) and ED1 ($p < 0.05$, up to 2 weeks).

DISCUSSION

In this study, we combined the fiber drawing process with conductive composite engineering to develop all-polymer miniaturized multifunctional probes for simultaneous optogenetic stimulation, neural recording, and delivery of viral vectors and pharmacological compounds into the mouse brain. Previously, diameters exceeding 400 μm for multifunctional thermally drawn probes were necessitated by comparatively large electrode dimensions designed to compensate for the poor electrical conductivity of commercially available polymer composites. The custom conductive polymer composite (gCPE) developed in this study was instrumental to reducing electrode dimensions and impedance, allowing for integration of higher density electrophysiology (6 electrodes), optical stimulation (a waveguide) and fluid delivery (2 channels) within probes with diameters <200 μm comparable to or smaller than those of silica fibers used for optogenetics. The flexibility and miniature footprint enhanced the biocompatibility of the probes as indicated by stable long-term recordings of isolated single-neuron action potentials as well as reduced glial response and blood-brain barrier breach 3 months after implantation.

We demonstrated the utility of the miniature and lightweight (<0.5 g) fiber probes by applying them to dynamic opto-electrophysiological study of ChR2 expression within individual brain regions and projection circuits. The latter was enabled by simultaneous implantations of multiple probes. Neural activity correlated with optical stimulation was found 11 days following viral delivery of ChR2 into the mPFC and BLA of wild type mice. In mice virally transduced with ChR2 in the BLA, the onset of optically-evoked neural activity in the vHPC was 11 days. In the BLA-to-mPFC projection optical responses were recorded 12 days following viral delivery into the BLA, and additional long-latency responses have emerged after 15 days. The observed differences in ChR2 expression in projections could in part be attributed to the proximity of the regions.

Functional expression of ChR2 was further confirmed in behaving mice through observation of increased locomotor activity during optical stimulation in the mPFC of animals virally

transduced in this region, as well as through observation of an anxiety phenotype arising during optical stimulation of an established BLA-to-vHPC projection, which could be counteracted by an injection of a synaptic blocker CNQX. Although a variety of approaches, such as optogenetics[32,33] and DREADD-facilitated behavioral modulation[34,35] combined with patch-clamp electrophysiology[36,37] in brain slices, are currently employed for functional projection mapping, these techniques do not permit direct correlation of circuit dynamics to observed behavioral outputs. By integrating dense neural recordings with the delivery of transgenes and optical stimuli within a miniature footprint, our device invites multi-site studies of neural projections to probe electrophysiological dynamics underlying a particular neurobiological process or a disease state.

Challenging backend connectorization is a common barrier for widespread neurotechnology adoption within the neuroscience community. Detailed hands-on instructions for connecting our multifunctional fibers to external headstages, light sources, and microinjection pumps (Supplementary Fig. 13) should enable straightforward assembly of the probes described here without the need for specialized equipment. This should enable a diversity of cell-type identification experiments in complex neural circuits[38], where one-step optogenetic capability would ensure one-to-one correspondence of optical and electrophysiological neural interrogation.

Methods

Synthesis of graphite-doped conductive polyethylene (gCPE)

Conductive polyethylene (CPE; Hillas Packaging) sheets were cut into 9 cm disks. Each disk was weighed and placed into a petri dish. Graphite particles (Sigma) were dissolved in the ethanol (70% by volume), and mixed by a vortex mixer and ultrasonicator. The solution was poured onto CPE sheets (5% graphite by weight relative to CPE), and dried overnight. Following drying disks were weighed again to confirm the graphite content. Several CPE sheets coated with graphite were stacked and consolidated in the hot press at 160 °C forming a "mille-feuille"-like structure. At high temperature, graphite particles get embedded within the bulk of molten CPE. The first consolidation step creates a heterogeneous CPE composite with non-uniform dispersion of graphite particles. To achieve uniform distribution of graphite within the gCPE composite, the consolidated material was cut into millimeter fragments and subjected to another consolidation step under pressure at 160–180 °C. The latter two steps were repeated 3 times, resulting in a gCPE composite with uniform graphite distribution and sheet resistance significantly lower than that of commercial CPE.

All-polymer multifunctional fiber fabrication

The fibers were produced by thermal drawing from macroscopic templates (preforms). To fabricate a preform, cyclic olefin copolymer (COC; TOPAS) sheets were rolled onto a 16 mm-thick polycarbonate (PC; Ajedium Films) rod, which was followed by several additional PC sheets. Eight rectangular grooves were machined within the outer PC layer, and six of the grooves were filled with gCPE electrodes. Additional COC sheets were wrapped around the structure, followed by several layers of PC that formed a sacrificial cladding that enabled stable processing conditions. The resulting preforms were consolidated under vacuum at

190 °C and then drawn at 240 °C using a custom-built fiber drawing tower as described in prior work[14].

Physical characterization of multifunctional fibers

The bending stiffness of the multifunctional fibers was measured by a dynamic mechanical analyzer (DMA, Q800, TA Instruments) in a single cantilever mode with 50 μm deformation amplitude within the frequency range 0.01–10 Hz. To quantify optical transmission losses, multifunctional fibers were coupled to a diode-pumped solid state (DPSS) laser (Laserglow, 50 mW maximum output, wavelength λ=473 nm) via ferrules and the light output was measured by photodetector (S121C, 400–1100 nm, 500 mW, Thorlabs) attached to power meter (PM100D, Thorlabs). Optical transmission was quantified for fiber length between 1–10 cm, bending angles 0°, 90°, 180°, and 270°, and radii of curvature 0.5, 1, 2.5, 5, 7.5, 10, 12.5, and 15 mm. Impedance of gCPE electrodes within fiber probes of lengths between 1–10 cm was measured by a LCR meter (HP4284A, Agilent Technologies) using a sinusoidal driving voltage (10 mV, 100 Hz ~ 10 kHz). Impedance spectra for gCPE electrodes were collected before and after a 24 hr soak in phosphate buffered saline (PBS). To characterize microfluidic channels, fiber probes were outfitted with external tubing and connected to the standard precision injection apparatus (NanoFil Syringe and UMP-3 Syringe pump, Word Precision Instruments). 10 μl of water was injected with at infusion speeds of 1, 10, 20, 50, 80, and 100 nl/s through the fiber channels, and injection rates were calculated by comparing input and output weight. The injection capability was also confirmed via infusion of the BlueJuice (10X, ThermoFisher Scientific) into 0.6% agarose gel at a speed of 100 nl/min.

Assembly of the multifunctional fiber-probes

The sacrificial PC layer was etched by immersion into dichloromethane (Sigma) for 1 min. To establish interfaces with embedded electrodes, the latter were exposed from the cladding manually, and silver paint (SPI Supplies) was used to connect the electrodes to the copper wires. The copper wires were wrapped around the fiber 20 min following the introduction of silver paint to allow for evaporation of the paint thinner. Connections to different electrodes were established at different locations along the fiber probe to avoid cross-talk. The wires were then soldered to the female pin connectors (Digi-Key). An insulated stainless steel ground wire was soldered to one of the pins. Finally, the entire electrode interface region of the fiber probe was coated with 5-min epoxy (Devcon) for mechanical stability and electrical insulation. For microfluidic interfaces, empty channels were exposed manually through the cladding and the entire region was placed within ethylene vinyl acetate tubing (0.5 mm inner diameter, McMaster-Carr) such that the fiber and the tubing were perpendicular to each other, allowing for fluid flow into microfluidic channels through the openings made in the cladding. The tubing was then affixed to the fiber with 5-min epoxy. Optical coupling was established by placing the uppermost part of the fiber into a 6.5 mm-long, 1.25 mm diameter zirconia ferrule (Thorlabs) and affixing it with optical epoxy (Thorlabs). The ferrule edge was then polished using a Thorlabs fiber polishing kit.

Implantation of fiber probes into mouse brain

All animal procedures were approved by the MIT Committee on Animal Care and carried out in accordance with the National Institutes of Health Guide for the Care and Use of

Laboratory Animals. Male C57BL/6 mice aged 6–8 weeks (Jackson Laboratory), and transgenic Thy1-ChR2-YFP mice (donated by G. Feng) aged 9–10 weeks were used for the study, and all surgeries were conducted under aseptic conditions. Mice were anaesthetized using via intraperitoneal (IP) injection of ketamine/xylazine mixture in saline (in mg/kg bodyweight: ketamine, 100; xylazine, 10), and then positioned in a stereotactic frame (David Kopf Instruments). A skin incision was made to expose the skull. Lambda and bregma points were used to align the skull with respect to the Mouse Brain Atlas[39]. All implantation and injection coordinates were established according to the brain atlas. The following three types of surgeries were performed: (a) a single injection/implantation in a medial prefrontal cortex (mPFC, coordinates relative to bregma; 1.7 mm anteroposterior (AP); 0.4 mm mediolateral (ML); −1.8 mm dorsoventral (DV)); (b) a viral injection/implantation of a fiber probe into basolateral amygdala (BLA, −1.6 mm AP; 3.2–3.4 mm ML; −4.9 mm DV) and a concomitant implantation of an identical fiber probe into mPFC (1.7 mm AP; 0.4 mm ML; −1.8 mm DV); (c) a viral injection/implantation of a fiber probe into BLA and a concomitant implantation of a fiber probe into ventral hippocampus (vHPC, −3.08 mm AP; 3.6–3.7 mm ML; −3.4 mm DV). Adeno-associated viruses serotype 5 (AAV5) carrying *CaMKIIa::hChR2(H134R)-eYFP* and *CaMKIIa::eYFP* plasmids were purchased from University of North Carolina Vector Core (Chapel Hill, NC) at concentrations of 2×10^{12} particles/mL and 3×10^{12} particles/mL respectively. Using a standard microinjection apparatus (NanoFil Syringe and UMP-3 Syringe pump, Word Precision Instruments) 0.5 μl of virus was injected through the microfluidic channels of implanted fiber probes at an infusion rate of 100 nl/min. During injections, the fiber-probes were raised 0.1 mm to accommodate the virus volume. The stainless steel ground wire was soldered to a miniature screw, which was affixed to the skull. Multifunctional probes were fixed to the skull with layer of adhesive (C&B Metabond; Parkell) and dental cement (Jet-Set 4, Lang Dental). Following the surgery and recovery, mice were single housed and were maintained at 22 °C and a 12 hour light/dark cycle and provided with food and water *ad libitum*.

In vivo electrophysiology

Multifunctional fiber-probes were attached to PZ2-32 head stage connected to RZ5D electrophysiology system (Tucker Davis Technologies, TDT). For optogenetic stimulation, a DPSS laser (Laserglow Technologies, 50 mW maximum power, wavelength λ = 473 nm) was air-coupled to a silica fiber patchcord, which was then connected to a fiber probe via a ferrule-to-ferrule coupling. For all experiments, pulsed stimulation with 5 ms pulse width was used. Frequencies of 10, 20, 100, 130 Hz were used. Stimulation was delivered in 1 s stimulation epochs separated by 1 s rest epochs. For the pharmacological experiments, 0.5 μl of CNQX solutions in phosphate buffered saline (PBS) with concentrations 0.01 mM, 0.05 mM, and 0.1 mM were injected using Nano Fil Syringe and UMP-3 micropump at a speed of 100 nl/min. Following recording, electrophysiological signal was digitized with 50 kHz sampling frequency and filtered in the frequency range 0.3–5 kHz. Spiking activity was detected using commercially available Offline Sorter software (Plexon) with a dead time of 1 ms. Following sorting, spikes were clustered in the first and second principal components (PC1-PC2) plane using k-means clustering, and L-ratios for each cluster were calculated using the same software. L-ratio < 0.05 is considered characteristic of well-isolated clusters[40]. Interspike intervals (ISI) were computed for every neuron, and histograms were

plotted by binning the intervals at 40 ms. Firing frequencies were calculated for each neuron by averaging the inverse values of ISIs.

Immunohistochemistry analyses of *c-fos* expression and foreign-body response

For c-fos quantification, mice transfected with *AAV5-CaMKIIa::hChR2(H134R)-eYFP* and *AAV5-CamKIIa::eYFP* were stimulated with 473 nm laser light (16 mW/mm^2, 20 Hz, 5 ms pulse width) for 3 minutes (1 s ON/OF epochs) and then kept in their home cages for 90 minutes to allow for c-fos expression. Mice were anesthetized via IP injection of Fatal Plus solution (100 mg/kg in saline), and transcardially perfused with 4% paraformaldehyde (PFA) in PBS. Brains were extracted and fixed in 4% PFA overnight, and then equilibrated in 30% sucrose in PBS. Samples were randomly allocated within each experimental group. The fixed brains were then sliced into 50 μm coronal sections using a vibrating blade microtome (Leica VT1000S). Sections were then permeabilized and blocked in 0.3% (vol/vol) Triton X-100 and 2.5% (vol/vol) goat serum in PBS for 1 hr. This was followed by a 20 hr incubation at 4 °C in a solution of primary antibodies (rabbit anti-c-fos[41] 1:500, Calbiochem, PC05) and 2.5% goat serum in PBS. Following incubation, the sections were washed 3 times for 30 min each with PBS. The slices were then incubated with secondary antibodies (Alexa Fluor 633 goat anti-rabbit 1:500, Life Technologies) for 2 hours at room temperature. Following 3 more washes with PBS, sections were incubated with a nuclear stain DAPI (4′6-diamidino-2-phenylindole) (1:50,000) for 30 min, and washed one more time. PVA-Dabco (Sigma) was used for mounting of slices onto glass microscope slides. A laser scanning confocal microscope (Fluoview FV1000, Olympus) with 4X (air, NA= 0.16), 20X (oil, NA = 0.85), and 60X (oil, NA = 1.42) objectives was used for image acquisition, and overview mosaic images were generated by FV1000 software (Olympus). ImageJ was used to quantify the number of c-fos positive cells in serial z-stack images with a depth of 10 μm. All imaging and analysis was blinded with respect to the experimental conditions. Long-term tissue responses to multimodal fiber probes and similarly sized stainless steel microwires (Good Fellow) were compared at 3 days, 2 weeks, 1 month, and 3 months. Fiber-probes and microwires were implanted to the mPFC region (1.7 AP; ±0.4 ML; −1.8 DV) of wild type mice (n = 8 per time point, 32 animals, each implanted with 1 fiber probe and 1 microwire). Perfusion, staining, and mounting procedures were identical to those described above with the exception of antibodies employed. The primary antibodies were used in the following concentrations: Goat anti-GFAP[42] 1:1000 (Abcam, ab53554); goat anti-Iba1[43] 1:500 (Abcam, ab107159); rabbit anti-CD68[44] 1:250 (Abcam, ab125212); donkey anti-mouse-IgG conjugated to Alexa Fluor 568[45] 1:1000 (ThermoFisher Scientific, A10037). Secondary antibodies were used in the following concentrations: donkey anti-goat labeled with Alexa Fluor 488 1:1000 (ThermoFisher Scientific, A11055); or donkey anti-rabbit labeled with Alex Flour 633 1:1000 (ThermoFisher Scientific, A21070). Confocal images were collected with an oil immersion 20X objective (NA = 0.85). Custom algorithm written in MATLAB (Mathworks) was used to quantify the fluorescence area corresponding to the presence of IgG, GFAP, Iba1, and ED1[46]. 360 radial lines separated by 1° were distributed from the center of the areas formerly occupied by implants, and the pixel intensity values were found along each line. Two boundary points were determined as 1σ standard deviation above average, and total coverage area was calculated within a 2-D outline of all end points (720, 2 per line).

Behavioral assays

Behavioral tests were performed by an investigator with knowledge of the identity of the experimental groups versus control groups. For each test, every implanted mouse was randomly allocated to an experimental group before a behavioral experiment. Open field tests (OFT) were conducted with wild type mice receiving optical stimulation coinciding with viral injection in the mPFC (*AAV5-CaMKIIa::hChR2(H134R)-eYFP* or *AAV5-CaMKIIa::eYFP* controls) as well as with wild type mice receiving optical stimulation in the mPFC or in the vHPC with the viruses delivered into the BLA (all implantations and injections are unilateral). For optical stimulation ($\lambda = 473$ nm, ~30 mW/mm^2 at the tip of the fiber, 20 Hz, 5 ms pulse width) was delivered through the fiber probes connected via ferrules to silica patch cords coupled to a DPSS laser (Laserglow Technologies). The 50×50 cm^2 open field chamber made of white plastic was virtually divided into the "center" (25×25 cm^2) and "periphery" fields. Mice in their home cages were brought into the room 2 hours prior to starting the experiments. Prior to starting the OFT, mice were placed in the center of the open field for 10 minutes to recover from handling stress. For *in vivo* pharmacological experiments, 0.5 µl of CNQX solution in PBS (0.1 mM) was injected via a fiber probe implanted in vHPC. OFT sessions consisted of three 3-minute epochs (OFF-ON-OFF stimulation, 9 min total), and all trials were recorded by a video camera. All experiments were conducted in the dark, under red light (intensity <10 lux, 650 nm wavelength) to minimize baseline stress associated with background lighting. EthoVision XT (Noldus) software was used for tracking of mouse position, and the location, distance traveled, speed, time spent in each region of the open field were calculated from the tracking data.

Statistical Analysis

MATLAB (Mathworks) software was used for assessing the statistical significance of all comparison studies in this work. For fiber characterization experiments, group sizes were determined by power analysis using the *sampsizepwr* function as implemented in the statistical toolbox ($\alpha = 0.05$, power = 0.9). Power analyses for predetermining sample sizes of immunohistochemistry and behavior test were not performed, instead the group sizes were chosen on the basis of previous research conducted in the same brain region or circuit[27, 30]. This was done to enable direct comparison of the observations with the prior work. For all parametric tests, data distribution was assumed to be normal, but this was not formally tested. In the statistical analysis for the characterization of impedance and light transmission, one-way ANOVA followed by Tukey's post-hoc comparison test were conducted with thresholds of *p < 0.05, **p < 0.01, ***p < 0.001. For the comparison between two groups in immunohistochemistry analyses and behavior assays, one-sided Student's t-tests were used, and significance threshold was placed at *p < 0.05, **p < 0.01. All error bars and shaded areas in the graphs represent standard deviation.

Supplementary Material

Refer to Web version on PubMed Central for supplementary material.

References

1. Boyden ES, Zhang F, Bamberg E, Nagel G, Deisseroth K. Millisecond-timescale, genetically targeted optical control of neural activity. Nat Neurosci. 2005; 8:1263–1268. [PubMed: 16116447]

2. Tye KM, Deisseroth K. Optogenetic investigation of neural circuits underlying brain disease in animal models. Nat Rev Neurosci. 2012; 13:251–266. [PubMed: 22430017]

3. Gradinaru V, Mogri M, Thompson KR, Henderson JM, Deisseroth K. Optical deconstruction of parkinsonian neural circuitry. Science. 2009; 324:354–359. [PubMed: 19299587]

4. Zhang F, Aravanis AM, Adamantidis A, de Lecea L, Deisseroth K. Circuit-breakers: optical technologies for probing neural signals and systems. Nat Rev Neurosci. 2007; 8:577–581. [PubMed: 17643087]

5. Aravanis AM, et al. An optical neural interface: in vivo control of rodent motor cortex with integrated fiberoptic and optogenetic technology. J Neural Eng. 2007; 4:S143. [PubMed: 17873414]

6. Minev IR, et al. Electronic dura mater for long-term multimodal neural interfaces. Science. 2015; 347:159–163. [PubMed: 25574019]

7. Park, SIl, et al. Soft, stretchable, fully implantable miniaturized optoelectronic systems for wireless optogenetics. Nat Biotechnol. 2015; 33:1280–1286. [PubMed: 26551059]

8. Jeong JW, et al. Wireless optofluidic systems for programmable in vivo pharmacology and optogenetics. Cell. 2015; 162:662–674. [PubMed: 26189679]

9. Ward MP, Rajdev P, Ellison C, Irazoqui PP. Toward a comparison of microelectrodes for acute and chronic recordings. Brain Res. 2009; 1282:183–200. [PubMed: 19486899]

10. Polikov VS, Tresco PA, Reichert WM. Response of brain tissue to chronically implanted neural electrodes. J Neurosci Methods. 2005; 148:1–18. [PubMed: 16198003]

11. Lind G, Linsmeier CE, Schouenborg J. The density difference between tissue and neural probes is a key factor for glial scarring. Sci Rep. 2013; 3

12. Abouraddy AF, et al. Towards multimaterial multifunctional fibres that see, hear, sense and communicate. Nat Mater. 2007; 6:336–347. [PubMed: 17471274]

13. Tao G, Stolyarov AM, Abouraddy AF. Multimaterial Fibers. Int J Appl Glas Sci. 2012; 3:349–368.

14. Canales A, et al. Multifunctional fibers for simultaneous optical, electrical and chemical interrogation of neural circuits in vivo. Nat Biotechnol. 2015; 33:277–284. [PubMed: 25599177]

15. Guimard NK, Gomez N, Schmidt CE. Conducting polymers in biomedical engineering. Polym Biomed Appl. 2007; 32:876–921.

16. Green RA, Lovell NH, Wallace GG, Poole-Warren LA. Conducting polymers for neural interfaces: Challenges in developing an effective long-term implant. Biomaterials. 2008; 29:3393–3399.

17. Kuo JTW, et al. Novel flexible Parylene neural probe with 3D sheath structure for enhancing tissue integration. Lab Chip. 2013; 13:554–561. [PubMed: 23160191]

18. Kim BJ, et al. 3D Parylene sheath neural probe for chronic recordings. J Neural Eng. 2013; 10:45002.

19. Huang JC. Carbon black filled conducting polymers and polymer blends. Adv Polym Technol. 2002; 21:299–313.

20. Roy N, Sengupta R, Bhowmick AK. Modifications of carbon for polymer composites and nanocomposites. Progress in Polymer Science. 2012; 37:781–819.

21. Mark JE. Polymer Data Handbook. J Am Chem Soc. 2009; 131:1250.

22. Bäumer, S. Handbook of Plastic Optics: Second Edition. Handbook of Plastic Optics: Second Edition. 2011.

23. Lee H, Bellamkonda RV, Sun W, Levenston ME. Biomechanical analysis of silicon microelectrode-induced strain in the brain. J Neural Eng. 2005; 2:81. [PubMed: 16317231]

24. Nagel G, et al. Channelrhodopsin-2, a directly light-gated cation-selective membrane channel. Proc Natl Acad Sci U S A. 2003; 100:13940–5. [PubMed: 14615590]

25. Flecknell, PA. Laboratory Animal Anaesthesia. Laboratory Animal Anaesthesia. 2009.

26. Cardin JA, et al. Targeted optogenetic stimulation and recording of neurons in vivo using cell-type-specific expression of Channelrhodopsin-2. Nat Protoc. 2010; 5:247–254. [PubMed: 20134425]

27. Anikeeva P, et al. Optetrode: a multichannel readout for optogenetic control in freely moving mice. Nat Neurosci. 2012; 15:163–170.

28. Bacon SJ, Headlam AJN, Gabbott PLA, Smith AD. Amygdala input to medial prefrontal cortex (mPFC) in the rat: a light and electron microscope study. Brain Res. 1996; 720:211–219. [PubMed: 8782914]

29. Lee BR, et al. Maturation of silent synapses in amygdala-accumbens projection contributes to incubation of cocaine craving. Nat Neurosci. 2013; 16:1644–1651. [PubMed: 24077564]

30. Felix-Ortiz AC, et al. BLA to vHPC inputs modulate anxiety-related behaviors. Neuron. 2013; 79:658–664. [PubMed: 23972595]

31. Saxena T, et al. The impact of chronic blood–brain barrier breach on intracortical electrode function. Biomaterials. 2013; 34:4703–4713. [PubMed: 23562053]

32. Gunaydin LA, et al. Natural neural projection dynamics underlying social behavior. Cell. 2014; 157:1535–1551. [PubMed: 24949967]

33. Desai M, et al. Mapping brain networks in awake mice using combined optical neural control and fMRI. J Neurophysiol. 2011; 105:1393–1405. [PubMed: 21160013]

34. Farrell MS, et al. A Gαs DREADD mouse for selective modulation of cAMP production in striatopallidal neurons. Neuropsychopharmacology. 2013; 38:854–62. [PubMed: 23303063]

35. Vardy E, et al. A New DREADD Facilitates the Multiplexed Chemogenetic Interrogation of Behavior. Neuron. 2015; 86:936–946. [PubMed: 25937170]

36. Nevian T, Larkum ME, Polsky A, Schiller J. Properties of basal dendrites of layer 5 pyramidal neurons: a direct patch-clamp recording study. Nat Neurosci. 2007; 10:206–14. [PubMed: 17206140]

37. Hunt RF, Girskis KM, Rubenstein JL, Alvarez-Buylla A, Baraban SC. GABA progenitors grafted into the adult epileptic brain control seizures and abnormal behavior. Nat Neurosci. 2013; 16:692–697. [PubMed: 23644485]

38. Kravitz AV, Tye LD, Kreitzer AC. Distinct roles for direct and indirect pathway striatal neurons in reinforcement. Nat Neurosci. 2012; 15:816–818. [PubMed: 22544310]

39. Paxinos, G., Franklin, KBJ. The mouse brain in stereotaxic coordinates. 2. Academic Press; 2004.

40. Schmitzer-Torbert N, Jackson J, Henze D, Harris K, Redish AD. Quantitative measures of cluster quality for use in extracellular recordings. Neuroscience. 2005; 131:1–11. [PubMed: 15680687]

41. Felix-Ortiz AC, Tye KM. Amygdala inputs to the ventral hippocampus bidirectionally modulate social behavior. J Neurosci. 2014; 34:586–95. [PubMed: 24403157]

42. Jukkola P, Guerrero T, Gray V, Gu C. Astrocytes differentially respond to inflammatory autoimmune insults and imbalances of neural activity. Acta Neuropathol Commun. 2013; 1:1–19.

43. Shi P, et al. Direct pro-inflammatory effects of prorenin on microglia. PLoS One. 2014; 9

44. Wes PD, et al. Tau overexpression impacts a neuroinflammation gene expression network perturbed in Alzheimer's disease. PLoS One. 2014; 9

45. Siracusa R, et al. The association of palmitoylethanolamide with luteolin decreases neuroinflammation and stimulates autophagy in Parkinson's disease model. CNS Neurol Disord Drug Targets. 2015; 14:1350–1366. [PubMed: 26295827]

46. Park S, et al. Optogenetic control of nerve growth. Sci Rep. 2015; 5
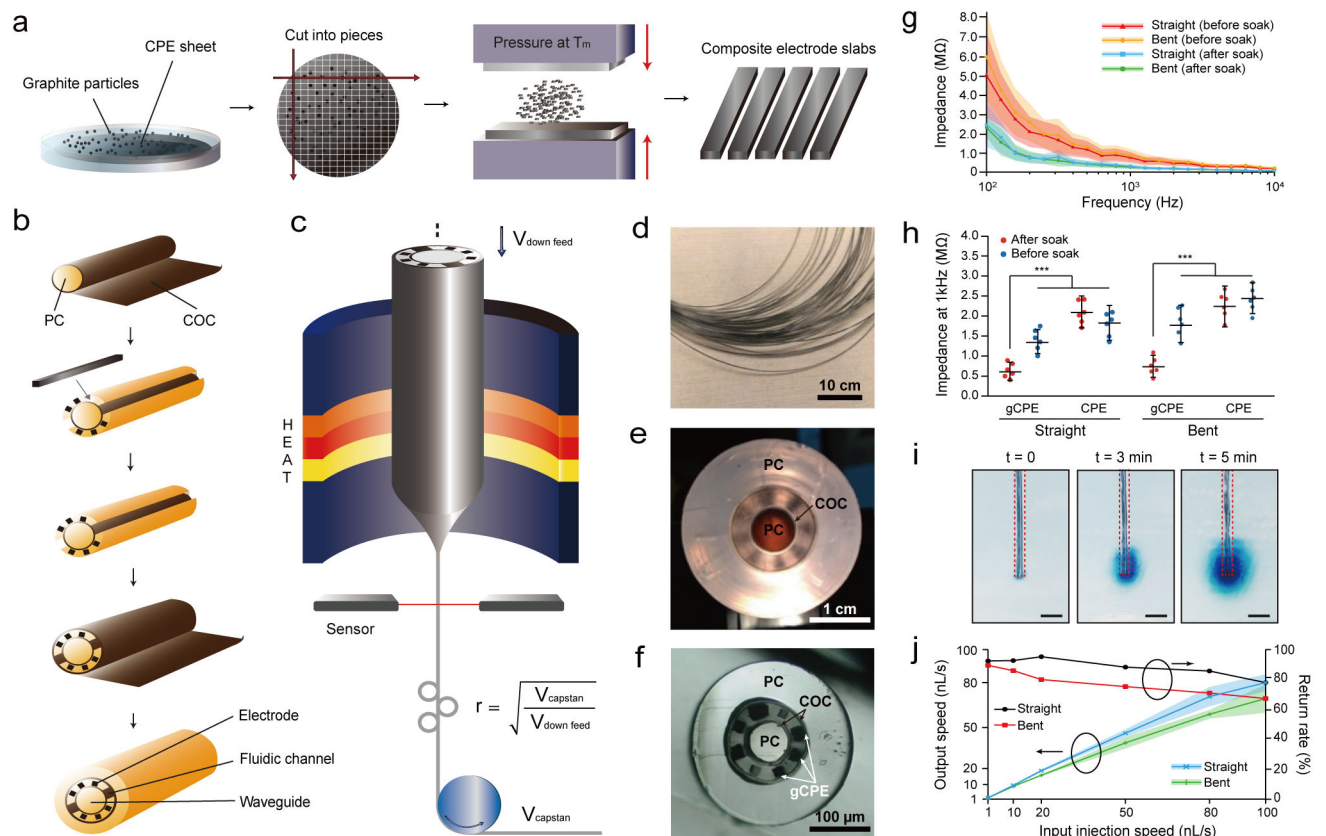
Figure 1. Fabrication and characterization of multifunctional fibers
(a) A schematic illustrating fabrication process for graphite-doped conductive polyethylene electrodes (gCPE). (b) Fabrication steps involved in assembly of the preform including a polycarbonate (PC) waveguide core, cyclic olefin copolymer (COC) cladding, gCPE electrodes, hollow channels, and protective sacrificial PC cladding. (c) An illustration of the fiber drawing process. The diameter of the resulting fiber is determined by the ratio of the capstan and feed speeds, and is monitored continuously during the process by a laser sensor. (d) Photograph of a bundle of fiber prior to etching of the sacrificial PC cladding. (e) Cross-sectional photograph of the preform prior to thermal drawing. (f) Cross-sectional microscope image of the multimodal fiber produced by thermal drawing of the preform in (e). (g, h) Impedance spectra of gCPE electrodes within the multimodal fiber. The impedance is reduced by 24 hr soak in phosphate buffered saline (PBS). Bending deformation (90°, 2.5 mm radius of curvature) does not appreciably alter impedance spectra. Number of samples n=6, ***$p < 0.001$ determined by one-way ANOVA. Flat: $p < 0.0001$, $F_{3, 20} = 27.42$, Bent: $p < 0.0001$, $F_{3, 20} = 21.86$. All error bars and shaded areas in the figure represent standard deviation. (i) Evaluation of microfluidic channels within multimodal fiber via infusion of a dye (BlueJuice) into a phantom brain (0.6% agarose gel). Images are taken at 0 min, 3 min, and 5 min after initiation of injection at a speed of 100 nl/min. Scale bar = 500 μm. (j) Output speed and return rate measured for microfluidic channel in multifunctional fiber. The microfluidic capability was only slightly reduced during 90° bending deformation. Number of samples n=6. Shaded areas represent standard deviation.
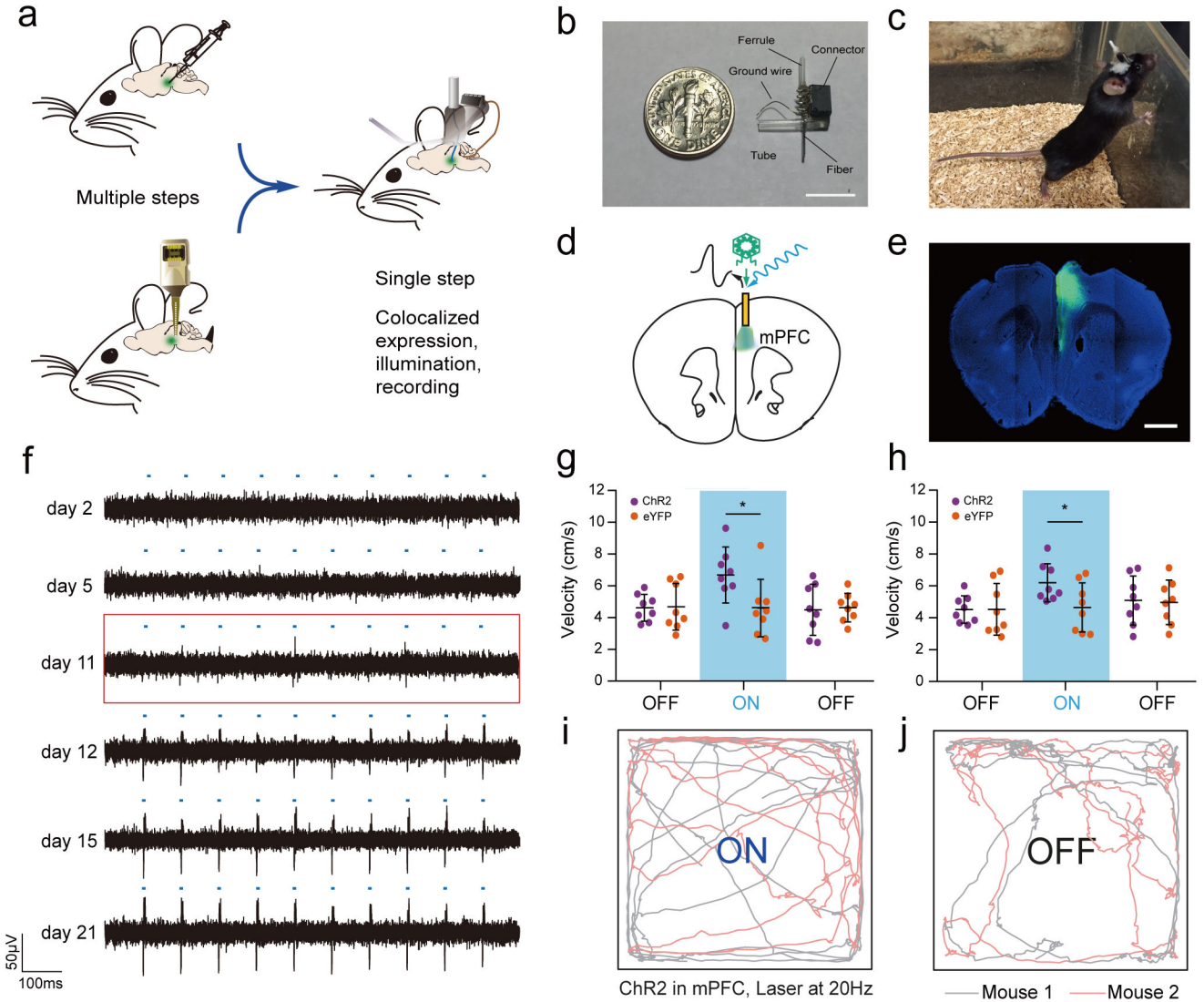
Figure 2. Multifunctional fiber probes enable viral delivery, optical stimulation, and recording with a one-step surgery

(a) A schematic comparing a traditional two-step surgery for optogenetic experiments and a one-step surgery enabled by a multifunctional fiber probe. (b) Picture of a multifunctional fiber probe outfitted with an optical ferrule, electrical connector, and an injection tube. The weight of the device varied between 0.3–0.5 g. Scale bar = 10 mm. (c) A wild-type mouse implanted with a multifunctional probe. (d) An illustration of viral delivery (*AAV5-CaMKIIα::ChR2-eYFP*), optical stimulation, and electrical recording in medial prefrontal cortex (mPFC) of wild-type mice with a fiber probe. (e) Expression of ChR2-eYFP in the mPFC for a wild-type (WT) mouse 2 weeks after viral transfection. Blue: DAPI, green: eYFP. Scale bar = 1 mm. (f) Electrophysiological recordings during optical stimulation in the mPFC using a fiber probe between 2 days and 21 days following transfection with AAV5-CaMKIIα::ChR2-eYFP. (10 Hz, 8.6 mW/mm^2, 5 ms pulse width). Optically evoked potentials were observed 11±2 days following implantation and injection surgery (orange box, n=8 mice). (g–j) Velocity recorded for WT mice implanted with fiber probes and

injected with *AAV5-CaMKIIa::ChR2-eYFP* (or control virus *AAV5-CaMKIIa::eYFP*) in mPFC during open field test (OFT). 9-min experiment consisted of 3-min epochs, OFF/ON/OFF optical stimulation: 5 ms pulse-width, power density 16 mW/mm^2, and frequency 20 Hz and 130 Hz. (g) 20Hz OFF_pre: $p = 0.9247$, $t = -0.0962$, ON: $p = 0.0352$, $t = 2.3309$, OFF_post: $p = 0.8279$, $t = -0.2215$. (h) 130Hz OFF_pre: $p = 0.9819$, $t = -0.023$, ON: $p = 0.0417$, $t = 2.2421$, OFF_post: $p = 0.8857$, $t = 0.1464$. d.f. = 14 for all. Error bars represent standard deviation (number of animals n=8, *p < 0.05; one-way student's t-test). (i–j) Representative trajectories for a ChR2 transfected mouse during (i) optical stimulation (5 ms pulse width, 20 Hz) ON and (j) OFF.
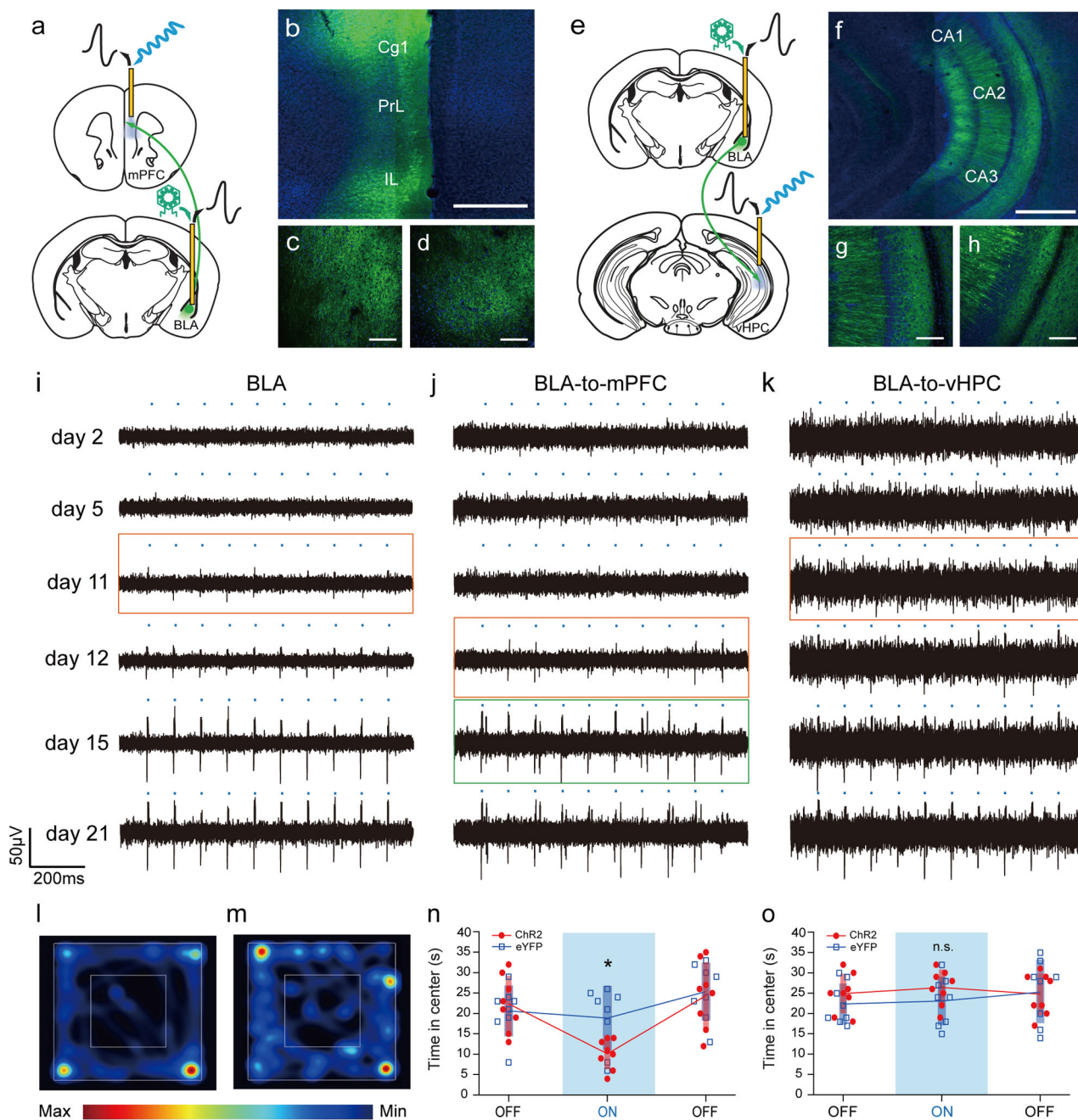
Figure 3. Optogenetic projection mapping using multimodal fiber probes
(a) An illustration of the basolateral amygdala (BLA) to mPFC projection. *AAV5-CaMKIIa::ChR2-eYFP* was delivered to BLA, and the optical stimulation and electrical recording were performed in the mPFC. (b–d) Confocal microscope images of a coronal section containing mPFC 6 weeks after viral transfection in the BLA. (c, d) Higher magnification images of prelymbic (PrL) and intralymbic (IL) areas of mPFC. Scale bars are (b) 500 μm and (c, d) 150 μm, respectively. (e) An illustration of the BLA to ventral hippocampus (vHPC) projection. Here virus was delivered to BLA, and the optical stimulation and electrical recording were performed in the vHPC. (f–h) Confocal

microscope images of a coronal section containing vHPC 6 weeks after viral transfection in the BLA. (g, h) Higher magnification images of CA2 and CA3 areas of vHPC. Scale bars are (f) 500 μm and (g, h) 150 μm, respectively. Blue: DAPI, green: eYFP. (i) Electrophysiological recording in the BLA during optical stimulation (10 Hz, 8.6 mW/mm^2, 5 ms pulse width) using a multifunctional fiber performed between 2 and 21 days following transfection with *AAV5-CaMKIIa::ChR2-eYFP*. Optically evoked potentials were observed 11±2 days (orange box, n=8 mice) following surgery. (j,k) Electrophysiological recordings during optical stimulation using multifunctional fibers implanted in the mPFC (j) and vHPC (k) between 2 and 21 days after viral transfection using fiber probes implanted in the BLA. Primary low-latency optically evoked potentials were observed following 12±1.4 days (orange box, n=8 mice) for mPFC (j) and following 11±2 days (orange box, n=8 mice) for vHPC (k). (j) For mPFC, secondary long-latency evoked potentials were recorded 15±2 days (green box, n=6 mice) after the surgery. (l–o) OFT experiments performed in mice implanted with multifunctional fiber probes in vHPC and BLA. 9-min OFT consisted of three 3-min epochs, OFF/ON/OFF optical stimulation (5 ms, 16 mW/mm^2, 20 Hz) in the vHPC. (l, m) Representative heatmap images tracing the position of a mouse transfected with ChR2 during (l) ON and (m) OFF optical stimulation epochs. (n) Time spent in the center of the open field for WT mice transfected in the BLA with *ChR2-eYFP* or *eYFP* alone in the absence or presence of optical stimulation in the vHPC. OFF_pre: p = 0.5957, t = 0.543, ON: p = 0.012, t = −2.8833, OFF_post: p = 0.7947, t = −0.2653. d.f. = 14 for all. (o) OFT identical to the one in (l–n) performed following delivery of synaptic blocker CNQX (0.1 mM, 0.5 μl) through a fiber probe implanted in vHPC. OFF_pre: p = 0.328, t = 1.0135, ON: p = 0.2319, t = 1.2497, OFF_post: p = 0.824, t = −0.2266. d.f. = 14 for all. Shaded areas represent standard deviation (Number of animals n=8, *p < 0.05; one way student's t-test).
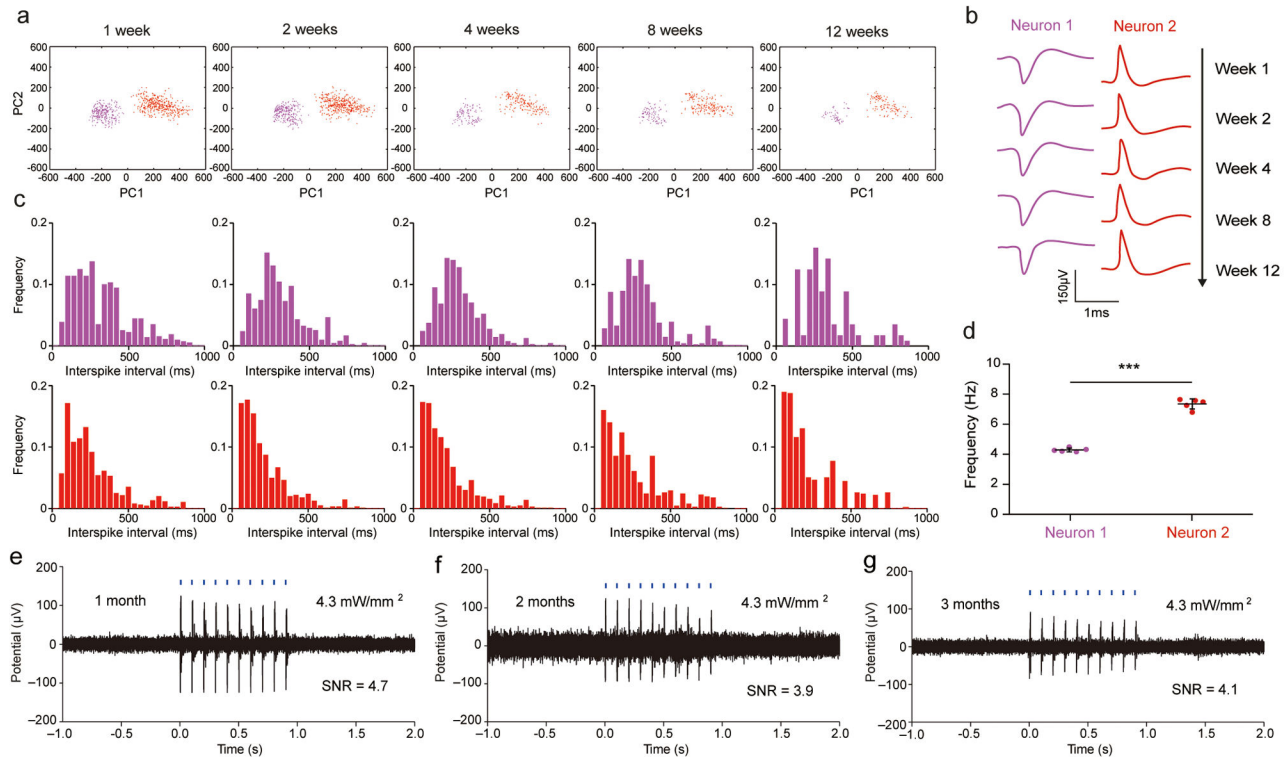
Figure 4. Investigation of single-unit potential with recorded signal from multimodal fiber device
(a–d) Tracking of isolated single neuron (unit) action potentials (spikes) recorded with a
with multifunctional fiber probe in mPFC over a period of 12 weeks following implantation.
(a) Clusters revealed by principle component analysis (PCA) of isolated action potentials.
(b) Average spike waveforms recorded between 1 and 12 weeks corresponding to clusters in
(a). (c) Interspike interval (ISI) histograms for isolated neurons 1 and 2 from (a,b).
Maximum histogram interval = 1000 ms and bin size = 40 ms. (d) Average firing
frequencies for neurons 1 and 2 obtained from ISI histograms. Significant difference
confirmed by one-way student's t-test ($p < 0.001$, $t = 18.7798$, d.f. = 8). Error bars represent
standard deviation (Number of samples n=5). (e–g) Electrophysiological recording of
optically evoked potentials in the mPFC of WT mice transfected with *AAV5-
CaMKIIa::ChR2-eYFP* performed (e) 1 month, (f) 2 months, and (g) 3 months after the
one-step implantation and transfection surgery. Optical stimulation parameters were fixed at
5 ms pulse width, frequency of 10 Hz and power density 4.3 mW/mm^2.
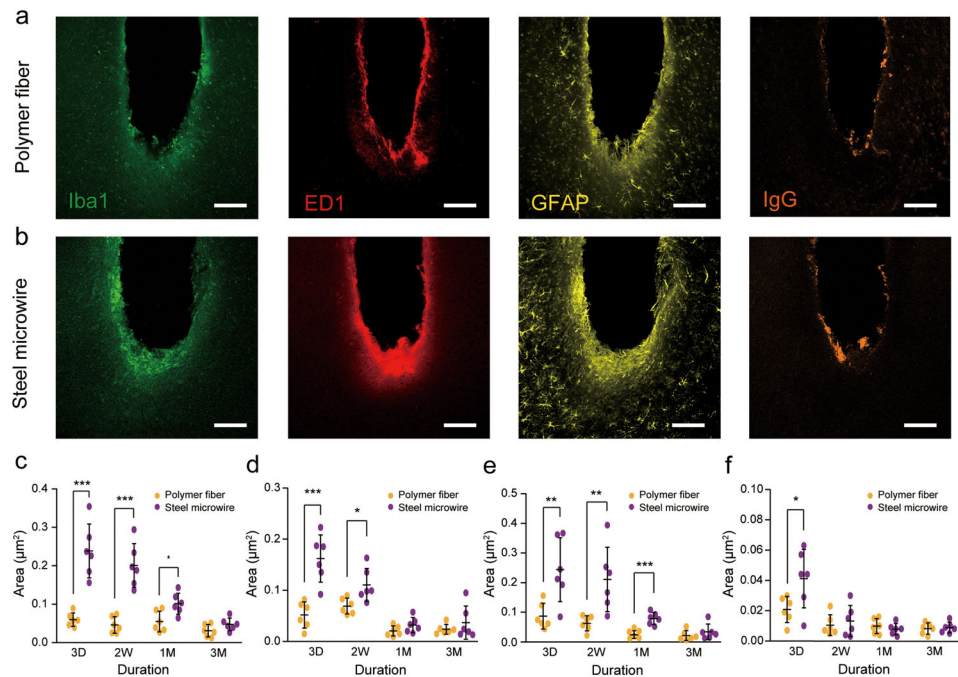
Figure 5. Evaluation of fiber probe and steel microwire biocompatibility using immunohistochemistry in coronal slices

(a, b) Representative confocal images of glial scarring and blood brain barrier breach surrounding (a) a 200 μm multifunctional fiber probe and (b) a 125 μm stainless steel microwire 1 month after implantation. Scale bar = 100 μm. (c–f) Average fluorescent intensity quantifying the presence of (c) Iba1, (d) ED1, (e) GFAP, and (f) IgG for fiber probes and microwires 3 days (3D), 2 weeks (2W), 1 month (1M), and 3 months (3M) following implantation. Iba1, 3 days: $p < 0.001$, $t = −6.0805$. 2 weeks: $p < 0.001$, $t = −6.1953$. 1 month: $p = 0.0144$, $t = −2.9547$. 3 months: $p = 0.1062$, $t = −1.7752$. ED1, 3 days: $p < 0.0001$, $t = −5.1123$. 2 weeks: $p = 0.0174$, $t = −2.8459$. 1 month: $p = 0.1462$, $t = −1.5756$. 3 months: $p = 0.37$, $t = −1.5756$. GFAP, 3 days: $p = 0.0079$, $t = −3.3081$. 2 weeks: $p = 0.0086$, $t = −3.2564$. 1 month: $p < 0.001$, $t = −5.5066$. 3 months: $p = 0.3508$, $t = −0.9787$. IgG, 3 days: $p = 0.0402$, $t = −2.3565$. 2 weeks: $p = −0.6106$, $t = −0.5256$. 1 month: $p = 0.4494$, $t = −0.7872$. 3 months: $p = 0.7569$, $t = −0.3182$. d.f. = 10 for all. Error bars represent standard deviation (Number of samples n=6 for each device and time point, *$p < 0.05$, **$p < 0.01$, ***$p < 0.001$; one way student's t-test).